Acta Astronautica 152 (2018) 740–751

Contents lists available at ScienceDirect

Acta Astronautica

journal homepage: www.elsevier.com/locate/actaastro

Attitude and vibration control with double-gimbal variable-speed control moment gyros

Takahiro Sasaki[a,*], Takashi Shimomura[a], Sam Pullen[b], Hanspeter Schaub[c]

[a] Osaka Prefecture University, 1-1 Gakuen, Sakai, Osaka, 599-8531, Japan
[b] Stanford University, Durand Bldg., Room 250, Stanford, CA, 94305-4035, USA
[c] University of Colorado, ECNT 321, 431 UCB, CO, 80309-0431, USA

ARTICLE INFO

Keywords:
Flexible spacecraft
DGVSCMG
Gain-scheduled control
LPV system
LMI
Dynamic inversion

ABSTRACT

The attitude and vibration control of a flexible spacecraft with two parallel double-gimbal variable-speed control moment gyros (DGVSCMGs) is considered. The coupled nonlinear equations of motion create a complex challenge in a pointing control development. First a Gain-Scheduled (GS) controller for a 3-axis attitude control is designed by the post-guaranteed linear matrix inequalities (LMIs) method with $\mathbf{H}_2/\mathbf{H}_\infty$ constraints. Next an $\mathbf{H}_2/\mathbf{H}_\infty$ controller for vibration control is designed to attain both attitude and vibration control at the same time. The two controllers are combined using the dynamic inversion (DI) technique. Finally, the effectiveness of the proposed combined controller is demonstrated through a numerical example.

1. Introduction

Both attitude and vibration control of a flexible spacecraft is of great interest in spacecraft applications. Missions of flexible spacecraft often require high speed attitude maneuvers and high pointing accuracy and stabilization. Increasing mission power requirements have created a trend in which recent communication satellites have large flexible solar battery paddles or communication antennas. For example, the Thermoelectric Outer Planets Spacecraft (TOPS) project [1,2] was developed by the National Aeronautics and Space Administration (NASA) to provide advanced systems technology that would allow realistic estimates of performance, cost, reliability, and scheduling that are required for an actual flight mission. The main antenna of TOPS has a diameter of 4.3 m. The Engineering Test Satellite VIII (ETS-VIII) [3], launched into Geo-synchronous orbit by the Japan Aerospace eXploration Agency (JAXA) in 2007, has large solar paddles as shown in Fig. 1. The main mission is mobile communication for which two large deployable reflectors (LDR) are appended in the roll axis direction. The dynamics between rigid spacecraft body and solar paddles are coupled each other.

JUNO [4], as illustrated in Fig. 2, is a NASA space probe orbiting Jupiter that was launched in 2011. The main mission is to measure Jupiter's composition, gravity field, magnetic field, and polar magnetosphere. JUNO has three solar panels that are symmetrically arranged. Two of the panels have four hinged segments each, and the third panel has three segments and a magnetometer. Each panel is 2.7 by 8.9 m long, and these panels are the biggest on any NASA deep-space probe. The mission requires high precision pointing that lasts about 3 h of perijove (periapsis of Jupiter) [5]. However, the flexing of the solar battery paddles or antennas due to engaging the orbit or attitude control mechanism make such mission pointing requirements very challenging to achieve. Additionally, inertia tensor modeling uncertainty of the flexible spacecraft is another challenge when providing precision pointing control. A pointing control solution for such a large spacecraft system with flexible components must account for these modeling uncertainties, as well as resulting dynamical disturbances due to flexing.

The attitude dynamics of a flexible spacecraft is time varying and nonlinear. It is impacted by orbital disturbances, model uncertainties and modal frequency of the flexible paddles or antennas. To guarantee robustness to these disturbances, uncertainties and flexibility, robust control theory is adopted, and it can deal with Linear Time-Invariant (LTI) systems with uncertainty. However, it is not appropriate for systems with drastic changes arising from nonlinearities or actuator motions in the original dynamics. Therefore, this paper investigates linear parameter-varying (LPV) control theory [6]. Using LPV control theory, the spacecraft dynamics are modeled as an LPV system which depends on the scheduling parameters to avoid difficulties arising from nonlinearities in the original dynamics. A gain-scheduled (GS) controller is applied to this model using linear matrix inequalities (LMIs). To solve LMIs simultaneously, a multi-objective GS controller for evaluating

* Corresponding author.
E-mail address: sasaki.takahiro@jaxa.jp (T. Sasaki).

https://doi.org/10.1016/j.actaastro.2018.08.047
Received 4 October 2017; Received in revised form 22 July 2018; Accepted 27 August 2018
Available online 12 September 2018

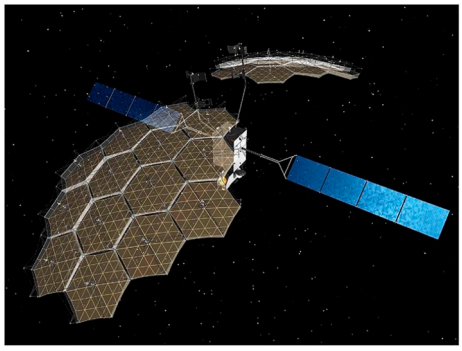

Fig. 1. ETS-VIII by JAXA [3].

Fig. 2. JUNO by NASA [5].

both optimality and robustness can be easily designed [7].

Conventionally, the LPV control theory introduces common Lyapunov functions [6,7] to guarantee overall stability as well as a desired control performance subject to a range of parameter changes of the LPV system. However, selecting a common Lyapunov function for the entire operating range leads to undesirable design conservatism. Many researchers have judged that this conservatism arises from selecting a common Lyapunov function and have shifted their research into parameter dependent Lyapunov functions [8,9], but the theory of these are more complicated and can add additional sufficiency conditions. In addition, changing rates of the system are restricted in many cases. To avoid these difficulties while mitigating conservatism, the post-guaranteed LMI method [10] is considered for flexible spacecraft attitude control in which distinct Lyapunov solutions are adopted. This paper adapts this post-guaranteed LMI method to the spacecraft attitude problem while using the dynamic inversion (DI) technique to achieve simultaneous attitude and vibration control.

Recently, DI-based control has gained popularity among engineers. This technique is often used for air borne objects such as aircraft [13,14] or missiles [15,16]. The concept of DI introduces an inversional representation and determines the control law by using both required command and inversional dynamics. This paper develops a new approach by adapting the DI technique to a flexible spacecraft with combined attitude and vibration controllers.

The attitude actuator considered in this paper is assumed to be a set of two parallel double-gimbal variable-speed control moment gyros (DGVSCMGs) [17,18] to attain high speed attitude maneuvers. A DGVSCMG is a new type of multi-degree-of-freedom (multi-DOF) actuator with several advantages. One DGVSCMG can generate large three-dimensional torques, which leads to a reduction of the number of actuators, the total mass, and volume allocation within the spacecraft. However, a wheel mechanical failure is a serious concern for a DGVSCMG device. Once its wheel has failed, a DGVSCMG is unable to generate any torque. To avoid such situations and provide robustness, it is convenient to introduce redundancy in the control devices.

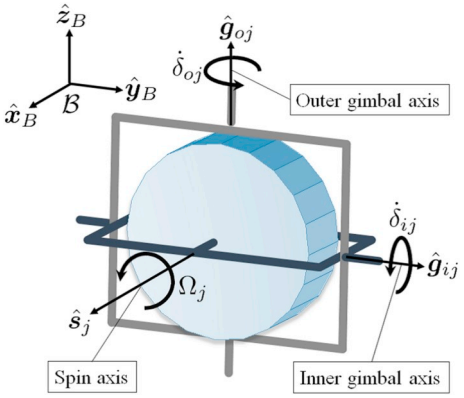

Fig. 3. *j*-th DGVSCMG.

DGVSCMGs have singularity configurations in which the Jacobian matrix is not invertible. In this paper, a singularity avoidance steering law is considered based on singularity robustness (SR) steering with null motion [19]. Finally, through numerical simulations, the effectiveness of the proposed combined controller for 3-axis attitude and vibration control and the singularity avoidance steering law is investigated.

2. Equation of motion

2.1. Nonlinear dynamics of a flexible spacecraft with DGVSCMGs

The spacecraft is assumed to be a flexible body and contains multiple DGVSCMG devices as modeled in Fig. 3. Note that the translational motion for the center of mass of the flexible structures is assumed to be negligibly small in the following analysis. The body-fixed frame $\mathscr{B}$ is represented by a set of unit vectors $\hat{\boldsymbol{x}}_B$, $\hat{\boldsymbol{y}}_B$, and $\hat{\boldsymbol{z}}_B$. The inertial frame is given by $\mathscr{N}$. Symbols $\mathscr{G}_o$, $\mathscr{G}_i$, and $\mathscr{W}$ denote the outer gimbal axis frame, the inner gimbal axis frame, and the wheel spin axis frame, respectively. Unit vectors $\hat{\boldsymbol{s}}_j$, $\hat{\boldsymbol{g}}_{ij}$, and $\hat{\boldsymbol{g}}_{oj}$ denote spin axis, inner/outer gimbal axis in *j*-th DGVSCMG, respectively.

Here, the equation of motion (EOM) of a flexible spacecraft with n DGVSCMGs is considered. The total inertial angular momentum $\boldsymbol{H}$ is described by

$$\boldsymbol{H} = \boldsymbol{H}_B + \boldsymbol{H}_{go} + \boldsymbol{H}_{gi} + \boldsymbol{H}_{ws} + \boldsymbol{H}_\eta \tag{1}$$

with

$$\boldsymbol{H}_B = [I_s]\boldsymbol{\omega}_{\mathscr{B}/\mathscr{N}} \tag{2a}$$

$$\boldsymbol{H}_{go} = [I_{go}] \sum_{j=1}^{n} \boldsymbol{\omega}_{\mathscr{G}oj/\mathscr{N}} \tag{2b}$$

$$\boldsymbol{H}_{gi} = [I_{gi}] \sum_{j=1}^{n} \boldsymbol{\omega}_{\mathscr{G}ij/\mathscr{N}} \tag{2c}$$

$$\boldsymbol{H}_{ws} = [I_{ws}] \sum_{j=1}^{n} \boldsymbol{\omega}_{\mathscr{W}j/\mathscr{N}} \tag{2d}$$

$$\boldsymbol{H}_\eta = \boldsymbol{Q}^T\dot{\boldsymbol{\eta}} \tag{2e}$$

where

$$\boldsymbol{\omega}_{\mathscr{G}oj/\mathscr{N}} = \boldsymbol{\omega}_{\mathscr{B}/\mathscr{N}} + \dot{\delta}_{oj}\hat{\boldsymbol{g}}_{oj} \tag{3a}$$

$$\boldsymbol{\omega}_{\mathscr{G}ij/\mathscr{N}} = \boldsymbol{\omega}_{\mathscr{B}/\mathscr{N}} + \dot{\delta}_{oj}\hat{\boldsymbol{g}}_{oj} + \dot{\delta}_{ij}\hat{\boldsymbol{g}}_{ij} \tag{3b}$$

$$\boldsymbol{\omega}_{\mathscr{W}j/\mathscr{N}} = \boldsymbol{\omega}_{\mathscr{B}/\mathscr{N}} + \dot{\delta}_{oj}\hat{\boldsymbol{g}}_{oj} + \dot{\delta}_{ij}\hat{\boldsymbol{g}}_{ij} + \Omega_j\hat{\boldsymbol{s}}_j \tag{3c}$$

and is the inertia tenso[I_s] r of a spacecraft (including the DGVSCMGs as point of masses) about the overall spacecraft center of mass and $\boldsymbol{\omega}_{\mathscr{B}/\mathscr{N}}$ is

the inertial angular velocity of the spacecraft. $[I_{gi}]$ and $[I_{go}]$ are the moment of inertia tensors of the DGVSCMG about the inner or outer gimbal axes respectively; $[I_{ws}]$ is the moment of inertia tensor of the wheel about the spin axes; and Ω_j is the j-th wheel spin rate, δ_{ij} or δ_{oj} is the inner or outer gimbal angle. In this flexible model, m elastic modes are considered, with $\boldsymbol{\eta} \in R^m$ the modal coordinate vector and $\boldsymbol{Q} \in R^{m\times 3}$ the coupling matrix between flexible and rigid dynamics. The total inertia tensor $[J]$ of a spacecraft including n DGVSCMGs is given by

$$[J] = [I_s] + [I_{go}] + [I_{gi}] + [I_{ws}]. \tag{4}$$

Note that ${}^{\mathscr{B}}[I_s]$, ${}^{\mathscr{G}_o}[I_{go}]$, ${}^{\mathscr{G}_i}[I_{gi}]$ and ${}^{\mathscr{G}_i}[I_{ws}]$ are constant matrices. The inertia tensor $[J]$ varies with time as seen by the body frame, since ${}^{\mathscr{B}}[I_{go}]$, ${}^{\mathscr{B}}[I_{gi}]$ and ${}^{\mathscr{B}}[I_{ws}]$ vary with time as follows:

$$\mathscr{B}_{[I_{go}]} = [\mathscr{B}\mathscr{G}_o]^{\mathscr{G}_o}[I_{go}][\mathscr{B}\mathscr{G}_o]^T \tag{5}$$

$$\mathscr{B}_{[I_{gi}]} = [\mathscr{B}\mathscr{G}_o][\mathscr{G}_o\mathscr{G}_i]^{\mathscr{G}_i}[I_{go}][\mathscr{G}_o\mathscr{G}_i]^T[\mathscr{B}\mathscr{G}_o]^T \tag{6}$$

$$\mathscr{B}_{[I_{ws}]} = [\mathscr{B}\mathscr{G}_o][\mathscr{G}_o\mathscr{G}_i]^{\mathscr{G}_i}[I_{ws}][\mathscr{G}_o\mathscr{G}_i]^T[\mathscr{B}\mathscr{G}_o]^T, \tag{7}$$

where the notation $[\mathscr{A}_1\mathscr{A}_2]$ defines the direction cosine matrix (DCM) that the $\mathscr{A}_2$ frame orientation is related to the $\mathscr{A}_1$ frame orientation. The rotation matrix $[\mathscr{A}_1\mathscr{A}_2]$ maps a vector with components taken in the $\mathscr{A}_2$ frame into a vector with components in the $\mathscr{A}_1$ frame. The EOM of a flexible spacecraft follows from Euler's equation:

$$\dot{\boldsymbol{H}} = \boldsymbol{L}, \tag{8}$$

where the vector $\boldsymbol{L}$ represents the sum of all the external torques experienced by the spacecraft. Substituting Eq. (1) into the LHS in Eq. (8) yields

$$\dot{\boldsymbol{H}}_B + \dot{\boldsymbol{H}}_{go} + \dot{\boldsymbol{H}}_{gi} + \dot{\boldsymbol{H}}_{ws} + \dot{\boldsymbol{H}}_{\eta} = \boldsymbol{L}. \tag{9}$$

In the following development, the shorthand notation $\boldsymbol{\omega} = \boldsymbol{\omega}_{\mathscr{B}/\mathscr{N}}$ is used to make the equation description more compact. Similarly, the definitions of the gimbal frame angular velocities and the wheel spin frame angular velocity definitions are shortened such as $\boldsymbol{\omega}_{\mathscr{G}_o/\mathscr{N}} = \boldsymbol{\omega}_{go}$, $\boldsymbol{\omega}_{\mathscr{G}_i/\mathscr{N}} = \boldsymbol{\omega}_{gi}$ and $\boldsymbol{\omega}_{\mathscr{W}/\mathscr{N}} = \boldsymbol{\omega}_{ws}$, respectively. Taking the inertial time derivative of the first term of the LHS in Eq. (9) leads to

$$\dot{\boldsymbol{H}}_B = [I_s]\dot{\boldsymbol{\omega}} + \boldsymbol{\omega}^{\times}[I_s]\boldsymbol{\omega}. \tag{10}$$

Note that the notation $\boldsymbol{x}^{\times}$ denotes the following skew-symmetric matrix:

$$\boldsymbol{x}^{\times} := \begin{bmatrix} 0 & -x_3 & x_2 \\ x_3 & 0 & -x_1 \\ -x_2 & x_1 & 0 \end{bmatrix}, \quad {}^{\forall}\boldsymbol{x} = [x_1\ x_2\ x_3]^T. \tag{11}$$

The second term of the LHS in Eq. (9) is related to the outer gimbals of the DGVSCMGs.

$$\dot{\boldsymbol{H}}_{go} = n[I_{go}]\dot{\boldsymbol{\omega}} + [I_{go}](\boldsymbol{G}_{go}\ddot{\boldsymbol{\delta}}_o + \boldsymbol{\omega}^{\times}(\boldsymbol{G}_{go}\dot{\boldsymbol{\delta}}_o)) + \sum_{j=1}^{n}\boldsymbol{\omega}_{goj}^{\times}([I_{go}]\boldsymbol{\omega}_{goj}), \tag{12}$$

where $\boldsymbol{\delta}_o = [\delta_{o1},...,\delta_{on}]^T \in R^n$ and $\boldsymbol{G}_{go} = [\hat{\boldsymbol{g}}_{o1},...,\hat{\boldsymbol{g}}_{on}] \in R^{3\times n}$ are the outer gimbal angle vector and the outer gimbal axes matrix, respectively. The third term of the LHS in Eq. (9) is related to the inner gimbals of the DGVSCMGs.

$$\dot{\boldsymbol{H}}_{gi} = n[I_{gi}]\dot{\boldsymbol{\omega}} + [I_{gi}](\boldsymbol{G}_{go}\ddot{\boldsymbol{\delta}}_o + \boldsymbol{G}_{gi}\ddot{\boldsymbol{\delta}}_i + \boldsymbol{\omega}^{\times}(\boldsymbol{G}_{go}\dot{\boldsymbol{\delta}}_o + \boldsymbol{G}_{gi}\dot{\boldsymbol{\delta}}_i) + (\boldsymbol{G}_{go}\dot{\boldsymbol{\delta}}_o)^{\times}\left(\boldsymbol{G}_{gi}\dot{\boldsymbol{\delta}}_i\right) + \sum_{j=1}^{n}\boldsymbol{\omega}_{gij}^{\times}\left([I_{gi}]\boldsymbol{\omega}_{gij}\right), \tag{13}$$

where $\boldsymbol{\delta}_i = [\delta_{i1},...,\delta_{in}]^T \in R^n$ and $\boldsymbol{G}_{gi} = [\hat{\boldsymbol{g}}_{i1},...,\hat{\boldsymbol{g}}_{in}] \in R^{3\times n}$ are the inner gimbal angle vector and the inner gimbal axes matrix, respectively. The fourth term of the LHS in Eq. (9) is related to the wheel spin rates of the DGVSCMGs.

$$\begin{aligned}\dot{\boldsymbol{H}}_{ws} = {} & n[I_{ws}]\dot{\boldsymbol{\omega}} + [I_{ws}](\boldsymbol{G}_{go}\ddot{\boldsymbol{\delta}}_o + \boldsymbol{G}_{gi}\ddot{\boldsymbol{\delta}}_i + \boldsymbol{G}_{ws}\dot{\boldsymbol{\Omega}} \\ & + \boldsymbol{\omega}^{\times}(\boldsymbol{G}_{go}\dot{\boldsymbol{\delta}}_o + \boldsymbol{G}_{gi}\dot{\boldsymbol{\delta}}_i + \boldsymbol{G}_{ws}\boldsymbol{\Omega}) + (\boldsymbol{G}_{go}\dot{\boldsymbol{\delta}}_o)^{\times}(\boldsymbol{G}_{gi}\dot{\boldsymbol{\delta}}_i + \boldsymbol{G}_{ws}\boldsymbol{\Omega}) \\ & + (\boldsymbol{G}_{gi}\dot{\boldsymbol{\delta}}_i)^{\times}(\boldsymbol{G}_{ws}\boldsymbol{\Omega})) + \sum_{j=1}^{n}\boldsymbol{\omega}_{wsj}^{\times}([I_{ws}]\boldsymbol{\omega}_{wsj}),\end{aligned} \tag{14}$$

where $\boldsymbol{\Omega} = [\Omega_1,...,\Omega_n]^T \in R^n$ is the wheel spin rate vector and $\boldsymbol{G}_{ws} = [\hat{\boldsymbol{s}}_1,...,\hat{\boldsymbol{s}}_n] \in R^{3\times n}$ is the matrix of the spin axes. The fifth term of the LHS in Eq. (9) is related to the flexible dynamics of a spacecraft.

$$\dot{\boldsymbol{H}}_{\eta} = \boldsymbol{Q}^T\ddot{\boldsymbol{\eta}} + \boldsymbol{\omega}^{\times}\boldsymbol{Q}^T\dot{\boldsymbol{\eta}}. \tag{15}$$

Finally, Eq. (9) is expanded to form the final spacecraft/DGVSCMGs kinetic equations of motion:

$$\begin{aligned}[J]\dot{\boldsymbol{\omega}} = {} & -[I_{go}](\boldsymbol{G}_{go}\ddot{\boldsymbol{\delta}}_o + \boldsymbol{\omega}^{\times}(\boldsymbol{G}_{go}\dot{\boldsymbol{\delta}}_o)) - [I_{gi}](\boldsymbol{G}_{go}\ddot{\boldsymbol{\delta}}_o + \boldsymbol{G}_{gi}\ddot{\boldsymbol{\delta}}_i \\ & + \boldsymbol{\omega}^{\times}(\boldsymbol{G}_{go}\dot{\boldsymbol{\delta}}_o + \boldsymbol{G}_{gi}\dot{\boldsymbol{\delta}}_i) + (\boldsymbol{G}_{go}\dot{\boldsymbol{\delta}}_o)^{\times}(\boldsymbol{G}_{gi}\dot{\boldsymbol{\delta}}_i)) \\ & - [I_{ws}](\boldsymbol{G}_{go}\ddot{\boldsymbol{\delta}}_o + \boldsymbol{G}_{gi}\ddot{\boldsymbol{\delta}}_i + \boldsymbol{G}_{ws}\dot{\boldsymbol{\Omega}} + \boldsymbol{\omega}^{\times}(\boldsymbol{G}_{go}\dot{\boldsymbol{\delta}}_o + \boldsymbol{G}_{gi}\dot{\boldsymbol{\delta}}_i + \boldsymbol{G}_{ws}\boldsymbol{\Omega}) \\ & + (\boldsymbol{G}_{go}\dot{\boldsymbol{\delta}}_o)^{\times}(\boldsymbol{G}_{gi}\dot{\boldsymbol{\delta}}_i + \boldsymbol{G}_{ws}\boldsymbol{\Omega}) + (\boldsymbol{G}_{gi}\dot{\boldsymbol{\delta}}_i)^{\times}(\boldsymbol{G}_{ws}\boldsymbol{\Omega})) - \boldsymbol{\omega}^{\times}[I_s]\boldsymbol{\omega} \\ & - \sum_{j=1}^{n}(\boldsymbol{\omega}_{wsj}^{\times}([I_{ws}]\boldsymbol{\omega}_{wsj}) + \boldsymbol{\omega}_{gij}^{\times}([I_{gi}]\boldsymbol{\omega}_{gij}) + \boldsymbol{\omega}_{goj}^{\times}([I_{go}]\boldsymbol{\omega}_{goj})) - \boldsymbol{Q}^T\ddot{\boldsymbol{\eta}} \\ & - \boldsymbol{\omega}^{\times}\boldsymbol{Q}^T\dot{\boldsymbol{\eta}} + \boldsymbol{L}.\end{aligned} \tag{16}$$

2.2. Modal equation of flexible structures

The modal equation for flexible structures of a spacecraft is described as follows:

$$\ddot{\boldsymbol{\eta}} + \boldsymbol{C}\dot{\boldsymbol{\eta}} + \boldsymbol{D}\boldsymbol{\eta} + \boldsymbol{Q}\dot{\boldsymbol{\omega}} = 0, \tag{17}$$

and the damping matrix $\boldsymbol{C}$ and the stiffness matrix $\boldsymbol{D}$ are given by

$$\boldsymbol{C} = \mathrm{diag}\{2\zeta_1\omega_{n1},...,2\zeta_1\omega_{nm}\} \tag{18}$$

$$\boldsymbol{D} = \mathrm{diag}\{\omega_{n1}^2,...,\omega_{nm}^2\}. \tag{19}$$

Note that ω_{ni} is the natural frequency, and ζ_i is the modal damping. $(1 \le i \le m)$

2.3. Kinematics

The quaternion set for attitude descriptions consists of a vector part and a scalar part. Given the principal rotation axis $\hat{\boldsymbol{\alpha}} = [\alpha_x\ \alpha_y\ \alpha_z]^T$ with $\hat{\boldsymbol{\alpha}}^T\hat{\boldsymbol{\alpha}} = 1$ and the rotation angle Θ, the quaternion (Euler Parameters) is (are) defined by

$$\boldsymbol{q} = \begin{bmatrix}\bar{\boldsymbol{q}} \\ q_4\end{bmatrix} := \begin{bmatrix}\hat{\boldsymbol{\alpha}}\sin\frac{\Theta}{2} \\ \cos\frac{\Theta}{2}\end{bmatrix}, \tag{20}$$

with the constraint:

$$\boldsymbol{q}^T\boldsymbol{q} = \hat{\boldsymbol{\alpha}}^T\hat{\boldsymbol{\alpha}}\sin^2\frac{\Theta}{2} + \cos^2\frac{\Theta}{2} = 1. \tag{21}$$

To formulate the attitude tracking problem of a spacecraft, the error quaternion $\boldsymbol{q}_e = \boldsymbol{q}_d^{\dagger}\boldsymbol{q}$ must be evaluted, where $\boldsymbol{q}$ denotes the current quaternion, $\boldsymbol{q}_d$ denotes the desired quaternion, and † refers to the conjugate operation. The kinematics equation is given by

$$\begin{bmatrix}\dot{\bar{\boldsymbol{q}}}_e \\ \dot{q}_{4e}\end{bmatrix} = \frac{1}{2}\boldsymbol{G}(\boldsymbol{q}_e)\boldsymbol{\omega}, \quad \boldsymbol{G}(\boldsymbol{q}_e) := \begin{bmatrix}q_{4e}\boldsymbol{I}_3 + \bar{\boldsymbol{q}}_e^{\times} \\ -\bar{\boldsymbol{q}}_e^T\end{bmatrix}. \tag{22}$$

2.4. LPV model for 3-axis attitude control

The spacecraft considered contains two parallel DGVSCMGs that have two parallel outer gimbal axes fixed to the spacecraft body depicted as in Fig. 4. In this case, the direction matrices in Eq. (16) are given by

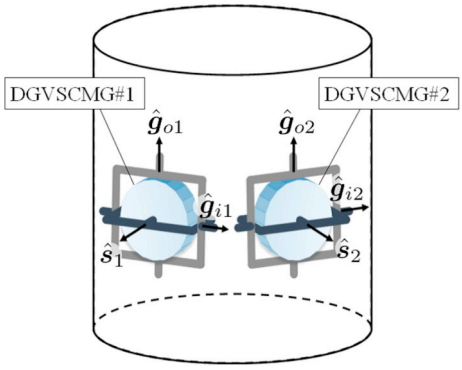

Fig. 4. Two parallel DGVSCMGs' allocation.

$$\boldsymbol{G}_{go} = \begin{bmatrix} 0 & 0 \\ 0 & 0 \\ 1 & 1 \end{bmatrix}, \quad \boldsymbol{G}_{gi} = \begin{bmatrix} -\sin\delta_{o1} & -\sin\delta_{o2} \\ \cos\delta_{o1} & \cos\delta_{o2} \\ 0 & 0 \end{bmatrix}, \quad \boldsymbol{G}_{ws} = \begin{bmatrix} \cos\delta_{i1}\cos\delta_{o1} & \cos\delta_{i2}\cos\delta_{o2} \\ \cos\delta_{i1}\sin\delta_{o1} & \cos\delta_{i2}\sin\delta_{o2} \\ -\sin\delta_{i1} & -\sin\delta_{i2} \end{bmatrix}. \tag{23}$$

Here, a linear parameter-varying (LPV) model for 3-axis attitude control is introduced. By using a Jacobian linearization of Eq. (16) around the equilibrium point ($\omega_{eeq} = 0$, $\dot{\boldsymbol{\Omega}}_{eq} = 0$, $\dot{\delta}_{ieq} = 0$, $\dot{\delta}_{oeq} = 0$) and the vector part in Eq. (22) around the equilibrium point ($\bar{\boldsymbol{q}}_e = 0$, $q_{4e} = 1$), the LPV model of a flexible spacecraft with DGVSCMGs is described as follows:

$$\dot{\omega} = \boldsymbol{A}(\rho)\omega + \boldsymbol{B}\boldsymbol{u} + \boldsymbol{E}w \tag{24}$$

$$\ddot{\bar{\boldsymbol{q}}}_e = \frac{1}{2}\boldsymbol{I}_3\omega \tag{25}$$

where

$$\boldsymbol{A}(\rho) = [J]^{-1}[I_{ws}](\rho)^{\times}, \tag{26}$$

$$\boldsymbol{B} = -[J]^{-1}[I_{ws}], \tag{27}$$

with

$$\rho = \boldsymbol{G}_s\boldsymbol{\Omega}, \tag{28}$$

$\boldsymbol{E}w$ is a disturbance term that includes the modal terms $\boldsymbol{Q}^T\ddot{\eta}$, $\omega^{\times}\boldsymbol{Q}^T\dot{\eta}$, the orbital disturbance term, and model error, such as uncertainty in the spacecraft inertia matrix $[\boldsymbol{J}]$. The control input $\boldsymbol{u}$ is given as follows:

$$\boldsymbol{u} = \bar{\boldsymbol{B}}\boldsymbol{u}' \tag{29}$$

with

$$\bar{\boldsymbol{B}} = [\boldsymbol{F}_{ws} \quad \boldsymbol{F}_{gi} \quad \boldsymbol{F}_{go}], \tag{30}$$

$$\boldsymbol{u}' = \begin{bmatrix} \dot{\boldsymbol{\Omega}} \\ \dot{\delta}_i \\ \dot{\delta}_o \end{bmatrix}, \tag{31}$$

where $\boldsymbol{u}'$ is the actuator input vector. This is called the steering law of DGVSCMGs. Using this steering law, the DGVSCMG system can avoid singularities. Note that the Jacobian matrix $\bar{\boldsymbol{B}}$ is constructed by

$$\boldsymbol{F}_{ws} = \begin{bmatrix} \cos\delta_{i1}\cos\delta_{o1} & \cos\delta_{i2}\cos\delta_{o2} \\ \cos\delta_{i1}\sin\delta_{o1} & \cos\delta_{i2}\sin\delta_{o2} \\ -\sin\delta_{i1} & -\sin\delta_{i2} \end{bmatrix},$$

$$\boldsymbol{F}_{ws} = \begin{bmatrix} \cos\delta_{i1}\cos\delta_{o1} & \cos\delta_{i2}\cos\delta_{o2} \\ \cos\delta_{i1}\sin\delta_{o1} & \cos\delta_{i2}\sin\delta_{o2} \\ -\sin\delta_{i1} & -\sin\delta_{i2} \end{bmatrix},$$

$$\boldsymbol{F}_{go} = \begin{bmatrix} -\Omega_1\cos\delta_{i1}\sin\delta_{o1} & -\Omega_2\cos\delta_{i2}\sin\delta_{o2} \\ \Omega_1\cos\delta_{i1}\cos\delta_{o1} & \Omega_2\cos\delta_{i2}\cos\delta_{o2} \\ 0 & 0 \end{bmatrix}.$$

Note that $\boldsymbol{F}_{ws}$, $\boldsymbol{F}_{gi}$ and $\boldsymbol{F}_{go}$ are the torque direction matrices of wheel spin rate, inner gimbal rotation and outer gimbal rotation, respectively.

Combining the linearlized dynamics in Eq. (24) and kinematics in Eq. (25), the state-space representation for 3-axis attitude control is given as follows:

$$\begin{bmatrix} \dot{\omega} \\ \dot{\bar{\boldsymbol{q}}}_e \end{bmatrix} = \begin{bmatrix} \boldsymbol{A}(\rho) & 0 \\ \frac{1}{2}\boldsymbol{I}_3 & 0 \end{bmatrix}\begin{bmatrix} \omega \\ \bar{\boldsymbol{q}}_e \end{bmatrix} + \begin{bmatrix} \boldsymbol{B} \\ 0 \end{bmatrix}\boldsymbol{u} + \begin{bmatrix} \boldsymbol{E} \\ 0 \end{bmatrix}\boldsymbol{w}. \tag{33}$$

Setting the state variable $\boldsymbol{x}$: $=[\omega_e^T \ \bar{\boldsymbol{q}}_e^T]^T$, the state-space representation of Eq. (33) is rewritten as follows:

$$\dot{\boldsymbol{x}} = \boldsymbol{A}_e(\rho)\boldsymbol{x} + \boldsymbol{B}_e\boldsymbol{u} + \boldsymbol{E}_e\boldsymbol{w}, \tag{34}$$

where

$$\boldsymbol{A}_e(\rho)\text{: } = \begin{bmatrix} \boldsymbol{A}(\rho) & 0 \\ \frac{1}{2}\boldsymbol{I}_3 & 0 \end{bmatrix},$$

$$\boldsymbol{B}_e\text{: } = \begin{bmatrix} \boldsymbol{B} \\ 0 \end{bmatrix},$$

$$\boldsymbol{E}_e\text{: } = \begin{bmatrix} \boldsymbol{E} \\ 0 \end{bmatrix}.$$

3. Controller synthesis

In this section, first an attitude controller for 3-axis attitude control is designed via LPV control theory. Then, the aimed attitude and vibration controller is constructed using dynamic inversion (DI).

3.1. Gain-scheduled attitude controller

A simple classical controller like a Lyapunov function-based controller always guarantees overall stability of attitude control. However, the closed-loop control performance is not necessarily acceptable. Therefore in this paper, an optimal GS controller for 3-axis attitude control is introduced to guarantee both overall stability and control performance and also robustness to orbital disturbances, model uncertainties and flexibility of the paddles or antennas. The generalized plant of Eq. (34) for control design is given as follows:

$$\begin{cases} \dot{\boldsymbol{x}} = \boldsymbol{A}_e(\rho)\boldsymbol{x} + \boldsymbol{B}_e\boldsymbol{u} + \boldsymbol{E}_e\boldsymbol{w} \\ \boldsymbol{z} = \bar{\boldsymbol{C}}\boldsymbol{x} + \bar{\boldsymbol{D}}\boldsymbol{u} \end{cases} \tag{36}$$

where the coefficient matrix set ($\bar{\boldsymbol{C}}$, $\bar{\boldsymbol{D}}$) is selected such that it satisfies the condition $\bar{\boldsymbol{C}}^T\bar{\boldsymbol{D}} = 0$, $\bar{\boldsymbol{D}}^T\bar{\boldsymbol{D}} > 0$, and where $\boldsymbol{w}$ and $\boldsymbol{z}$ are the disturbance input vector and the performance output vector for the LPV model in Eq. (34), respectively. For this plant, the state-feedback GS controller:

$$\boldsymbol{u} = -\boldsymbol{K}(\rho)\boldsymbol{x} \tag{37}$$

is designed. With full state feedback using the designed attitude controller, the angular velocity of the spacecraft, the inner/outer gimbal angles, and the wheel spin rates are needed to determine the required input, and these measurements can be provided by the gyro sensor (or estimated value coming from a Kalman filter) and tachometers in the actuators. The LPV model and the GS controller are expressed by the following polytopic representation:

$$\boldsymbol{A}_e(\rho) = \sum_{i=1}^{p} \lambda_i(\rho)\boldsymbol{A}_{ei}, \tag{38}$$

$$\boldsymbol{K}(\rho) = \sum_{i=1}^{p} \lambda_i(\rho)\boldsymbol{K}_i, \tag{39}$$

$$\lambda_i(\rho) \geq 0, \ \sum_{i=1}^{p} \lambda_i(\rho) = 1, \tag{40}$$

where p denotes the number of vertices, in this case, p is equal to 8 (=2^3). λ is the polytopic coefficient. Details regarding the determination of λ are described in Ref. [20]. The matrices $\boldsymbol{A}_{ei}$ and $\boldsymbol{K}_i$ are determined by the combination of the maximum and minimum values of the scheduling parameters ρ parameterized by δ_o, δ_i, and Ω. Note that the spacecraft inertia matrix $[\boldsymbol{J}]$ is assumed to be the initial condition as a constant matrix in the controller design. Let us introduce the following mixed $\mathbf{H}_2/\mathbf{H}_\infty$ LMI problem [7]:

$$\inf_{\boldsymbol{W}_i, \boldsymbol{X}, \boldsymbol{Z}} [\text{Trace}(\boldsymbol{Z})] \quad \text{subject to} \tag{41a}$$

$$\Psi_{H2} > 0, \quad \Psi'_{H2i} < 0, \tag{41b}$$

$$\Psi_{H\infty i} < 0, \tag{41c}$$

for all $1 \leq i \leq p$,

where

$$\Psi_{H2} = \begin{bmatrix} \boldsymbol{X} & * \\ \boldsymbol{E}_e^T & \boldsymbol{Z} \end{bmatrix},$$

$$\Psi'_{H2i} = \begin{bmatrix} (\boldsymbol{A}_{ei}\boldsymbol{X} - \boldsymbol{B}_e\boldsymbol{W}_i) + (\bullet)^T & * \\ \bar{\boldsymbol{C}}\boldsymbol{X} - \bar{\boldsymbol{D}}\boldsymbol{W}_i & -\boldsymbol{I} \end{bmatrix},$$

$$\Psi_{H\infty i} = \begin{bmatrix} (\boldsymbol{A}_{ei}\boldsymbol{X} - \boldsymbol{B}_e\boldsymbol{W}_i) + (\bullet)^T & * & * \\ \bar{\boldsymbol{C}}\boldsymbol{X} - \bar{\boldsymbol{D}}\boldsymbol{W}_i & -\gamma\boldsymbol{I} & * \\ \boldsymbol{E}_e^T & 0 & -\gamma\boldsymbol{I} \end{bmatrix},$$

Eqs. (41a) and (41b) guarantee the $\mathscr{H}_2$ performance, and Eq. (41c) gives the $\mathbf{H}_\infty$ constraint. Using the optimal solution set ($\boldsymbol{X}$, $\boldsymbol{W}_i$) solving the $\mathbf{H}_2$ and $\mathbf{H}_\infty$ problems simultaneously in Eq. (41), the extreme controllers $\boldsymbol{K}_i$ at each vertex of the operation range are given by

$$\boldsymbol{K}_i = \boldsymbol{W}_i\boldsymbol{X}^{-1}, \quad 1 \leq i \leq p. \tag{42}$$

Then, the GS controller is constructed by substituting Eq. (42) into Eq. (39). Note that the common Lyapunov solution $\boldsymbol{X} > 0$ was used in past GS controller design and resulted in conservatism. As an alternative, the post-guaranteed LMI method [10] is used, in which the distinct Lyapunov solutions $\boldsymbol{X}_i > 0$ are adopted. By using this method, the mixed $\mathbf{H}_2/\mathbf{H}_\infty$ LMI problem can be described as follows:

$$\inf_{\boldsymbol{W}_i, \boldsymbol{X}_i, \boldsymbol{Z}_i} [\text{Trace}(\boldsymbol{Z}_i)] \quad \text{subject to} \tag{43a}$$

$$\widetilde{\Psi}_{H2i} > 0, \quad \widetilde{\Psi}'_{H2i} < 0, \tag{43b}$$

$$\widetilde{\Psi}_{H\infty i} < 0, \tag{43c}$$

for each $1 \leq i \leq p$,

where

$$\widetilde{\Psi}_{H2i} = \begin{bmatrix} \boldsymbol{X}_i & * \\ \boldsymbol{E}_e^T & \boldsymbol{Z}_i \end{bmatrix}$$

$$\widetilde{\Psi}'_{H2i} = \begin{bmatrix} (\boldsymbol{A}_{ei}\boldsymbol{X}_i - \boldsymbol{B}_e\boldsymbol{W}_i) + (\bullet)^T & * \\ \bar{\boldsymbol{C}}\boldsymbol{X}_i - \bar{\boldsymbol{D}}\boldsymbol{W}_i & -\boldsymbol{I} \end{bmatrix}$$

$$\widetilde{\Psi}_{H\infty i} = \begin{bmatrix} (\boldsymbol{A}_{ei}\boldsymbol{X}_i - \boldsymbol{B}_e\boldsymbol{W}_i) + (\bullet)^T & * & * \\ \bar{\boldsymbol{C}}\boldsymbol{X}_i - \bar{\boldsymbol{D}}\boldsymbol{W}_i & -\gamma\boldsymbol{I} & * \\ \boldsymbol{E}_e^T & 0 & -\gamma\boldsymbol{I} \end{bmatrix}.$$

Using the optimal solution set ($\boldsymbol{X}_i$, $\boldsymbol{W}_i$) to the problem of Eq. (43), less conservative extreme controllers can be obtained. These extreme controllers are given by

$$\boldsymbol{K}_i = \boldsymbol{W}_i\boldsymbol{X}_i^{-1}, \quad 1 \leq i \leq p. \tag{44}$$

By using these extreme controllers, a GS controller is again constructed as in Eq. (39). In order to guarantee overall stability and control performance over the entire operational range, we seek a common Lyapunov solution $\boldsymbol{X}_c > 0$ that satisfies the following LMIs [10]:

$$\inf_{\boldsymbol{X}_c, \boldsymbol{Z}} [\text{Trace}(\boldsymbol{Z})] \quad \text{subject to} \tag{45a}$$

$$\overline{\Psi}_{H2c} > 0, \quad \overline{\Psi}_{H2i} < 0, \tag{45b}$$

$$\overline{\Psi}_{H\infty i} < 0, \tag{45c}$$

for all $1 \leq i \leq p$,

where

$$\overline{\Psi}_{H2c} = \begin{bmatrix} \boldsymbol{X}_c & * \\ \boldsymbol{E}^T & \boldsymbol{Z} \end{bmatrix},$$

$$\overline{\Psi}'_{H2i} = \begin{bmatrix} (\boldsymbol{A}_{ei} - \boldsymbol{B}_e\boldsymbol{K}_i)\boldsymbol{X}_c + (\bullet)^T & * \\ (\bar{\boldsymbol{C}} - \bar{\boldsymbol{D}}\boldsymbol{K}_i)\boldsymbol{X}_c & -\boldsymbol{I} \end{bmatrix},$$

$$\overline{\Psi}_{H\infty i} = \begin{bmatrix} (\boldsymbol{A}_{ei} - \boldsymbol{B}_e\boldsymbol{K}_i)\boldsymbol{X}_c + (\bullet)^T & * & * \\ (\bar{\boldsymbol{C}} - \bar{\boldsymbol{D}}\boldsymbol{K}_i)\boldsymbol{X}_c & -\gamma\boldsymbol{I} & * \\ \boldsymbol{E}_e^T & 0 & -\gamma\boldsymbol{I} \end{bmatrix}.$$

3.2. Attitude and vibration controller

To attain both attitude and vibration control, a vibration controller is designed. From Eq. (17), the state-space representation for vibration control is given as follows:

$$\begin{bmatrix} \ddot{\boldsymbol{\eta}} \\ \dot{\boldsymbol{\eta}} \end{bmatrix} = \begin{bmatrix} -\boldsymbol{C} & -\boldsymbol{D} \\ \boldsymbol{I} & 0 \end{bmatrix} \begin{bmatrix} \dot{\boldsymbol{\eta}} \\ \boldsymbol{\eta} \end{bmatrix} + \begin{bmatrix} -\boldsymbol{Q} \\ 0 \end{bmatrix} \dot{\boldsymbol{\omega}} + \begin{bmatrix} \widetilde{\boldsymbol{E}} \\ 0 \end{bmatrix} \widetilde{\boldsymbol{w}} \tag{46}$$

or

$$\dot{\widetilde{\boldsymbol{x}}} = \widetilde{\boldsymbol{A}}_e\widetilde{\boldsymbol{x}} + \widetilde{\boldsymbol{B}}_e\dot{\boldsymbol{\omega}} + \widetilde{\boldsymbol{E}}_e\widetilde{\boldsymbol{w}}, \tag{47}$$

where

$$\widetilde{\boldsymbol{x}} := [\dot{\boldsymbol{\eta}}^T \ \boldsymbol{\eta}^T]^T \tag{48}$$

with

$$\widetilde{\boldsymbol{A}}_e := \begin{bmatrix} -\boldsymbol{C} & -\boldsymbol{D} \\ \boldsymbol{I} & 0 \end{bmatrix}, \quad \widetilde{\boldsymbol{B}}_e := \begin{bmatrix} -\boldsymbol{Q} \\ 0 \end{bmatrix}, \quad \widetilde{\boldsymbol{E}}_e := \begin{bmatrix} \widetilde{\boldsymbol{E}} \\ 0 \end{bmatrix}. \tag{49}$$

The generalized plant for Eq. (47) is defined as follows:

$$\begin{cases} \dot{\widetilde{\boldsymbol{x}}} = \widetilde{\boldsymbol{A}}_e\widetilde{\boldsymbol{x}} + \widetilde{\boldsymbol{B}}_e\dot{\boldsymbol{\omega}} + \widetilde{\boldsymbol{E}}_e\widetilde{\boldsymbol{w}} \\ \widetilde{\boldsymbol{z}} = \widetilde{\boldsymbol{C}}\widetilde{\boldsymbol{x}} + \widetilde{\boldsymbol{D}}\dot{\boldsymbol{\omega}} \end{cases} \tag{50}$$

where the coefficient matrix set ($\widetilde{\boldsymbol{C}}$, $\widetilde{\boldsymbol{D}}$) is selected such that it satisfies the condition $\widetilde{\boldsymbol{C}}^T\widetilde{\boldsymbol{D}} = 0$, $\widetilde{\boldsymbol{D}}^T\widetilde{\boldsymbol{D}} > 0$, and where $\widetilde{\boldsymbol{w}}$ and $\widetilde{\boldsymbol{z}}$ are the disturbance input vector and the performance output vector for the LPV model in Eq. (47), respectively. For this plant, the state-feedback GS controller:

$$\dot{\boldsymbol{\omega}} = -\widetilde{\boldsymbol{K}}\widetilde{\boldsymbol{x}} \tag{51}$$

is designed. Let us introduce the following mixed $\mathbf{H}_2/\mathbf{H}_\infty$ LMI problem again to guarantee the robustness to parameter perturbations (such as model error of the paddle or antenna and sensor error) as follows:

$$\inf_{\widetilde{\boldsymbol{W}}, \widetilde{\boldsymbol{X}}, \widetilde{\boldsymbol{Z}}} [\text{Trace}(\widetilde{\boldsymbol{Z}})] \quad \text{subject to} \tag{52a}$$

$$\overline{\Psi}_{H2} > 0, \quad \overline{\Psi}_{H2} < 0, \tag{52b}$$

$$\overline{\Psi}_{H\infty} < 0, \tag{52c}$$

where

$$\overline{\Psi}_{H2} = \begin{bmatrix} \widetilde{\boldsymbol{X}} & * \\ \widetilde{\boldsymbol{E}}_e^T & \widetilde{\boldsymbol{Z}} \end{bmatrix},$$

$$\overline{\Psi}_{H2} = \begin{bmatrix} (\widetilde{\boldsymbol{A}}_e\widetilde{\boldsymbol{X}} - \widetilde{\boldsymbol{B}}_e\widetilde{\boldsymbol{W}}) + (\bullet)^T & * \\ \widetilde{\boldsymbol{C}}\widetilde{\boldsymbol{X}} - \widetilde{\boldsymbol{D}}\widetilde{\boldsymbol{W}} & -\boldsymbol{I} \end{bmatrix},$$

$$\overline{\Psi}_{H\infty} = \begin{bmatrix} (\widetilde{\boldsymbol{A}}_e\widetilde{\boldsymbol{X}} - \widetilde{\boldsymbol{E}}_e\widetilde{\boldsymbol{W}}) + (\bullet)^T & * & * \\ \widetilde{\boldsymbol{C}}\widetilde{\boldsymbol{X}} - \widetilde{\boldsymbol{D}}\widetilde{\boldsymbol{W}} & -\gamma\boldsymbol{I} & * \\ \widetilde{\boldsymbol{E}}_e^T & 0 & -\gamma\boldsymbol{I} \end{bmatrix}.$$

Using the optimal solution set $\widetilde{\boldsymbol{X}}$, $\widetilde{\boldsymbol{W}}$, the optimal controller $\widetilde{\boldsymbol{K}}$ is given by

$$\widetilde{\boldsymbol{K}} = \widetilde{\boldsymbol{W}}\widetilde{\boldsymbol{X}}^{-1}. \tag{53}$$

Note that in Eq. (50), the control input given by $\dot{\omega}$ is the differential of the upper part of the state vector in the generalized plant for attitude control in Eq. (36). However, the differential of the angular velocity $\dot{\omega}$ is generally not available as a control input. To utilize this parameter as a control input, we use the DI technique [13–16]. Using the desired angular acceleration $\dot{\omega}_{\text{ref}}$ coming from the vibration controller in Eq. (51), the desired control input for vibration control $\boldsymbol{u}_v$ is to be given by the following DI system:

$$\boldsymbol{u}_v = \boldsymbol{B}^{-1}(\dot{\omega}_{\text{ref}} - \boldsymbol{A}(\rho)\omega), \tag{54}$$

which is derived from Eq. (24). Combining the GS attitude controller in Eq. (37) and the vibration controller in Eq. (54), the attitude and vibration controller $\tilde{\boldsymbol{u}}$ is given by

$$\tilde{\boldsymbol{u}} = \boldsymbol{u} + \overline{\boldsymbol{W}}\boldsymbol{u}_v, \tag{55}$$

where the weighting matrix $\overline{\boldsymbol{W}}$ is given by

$$\overline{\boldsymbol{W}} = \text{diag}\{g_1, g_2, g_3\}, \quad g_i > 0, \quad 1 \le i \le 3. \tag{56}$$

Substituting Eqs. (37) and (54) into Eq. (55), while substituting Eq. (51) into Eq. (54), the controller in Eq. (55) to attain both attitude and vibration control can be rewritten as

$$\tilde{\boldsymbol{u}} = -(\boldsymbol{K}_d(\rho) + \overline{\boldsymbol{W}}\boldsymbol{B}^{-1}\boldsymbol{A}(\rho))\omega - \boldsymbol{K}_p(\rho)\overline{\boldsymbol{q}}_e - \overline{\boldsymbol{W}}\boldsymbol{B}^{-1}(\widetilde{\boldsymbol{K}}_p\eta + \widetilde{\boldsymbol{K}}_d\dot{\eta}), \tag{57}$$

where

$$\boldsymbol{K}(\rho) = [\boldsymbol{K}_d(\rho)\ \ \boldsymbol{K}_p(\rho)], \quad \widetilde{\boldsymbol{K}} = [\widetilde{\boldsymbol{K}}_d\ \ \widetilde{\boldsymbol{K}}_p] \tag{58}$$

with $\boldsymbol{K}_d(\rho) \in R^{3\times3}$, $\boldsymbol{K}_p(\rho) \in R^{3\times3}$, $\widetilde{\boldsymbol{K}}_d \in R^{3\times3}$ and $\widetilde{\boldsymbol{K}}_p \in R^{3\times3}$. With full state feedback using the designed attitude and vibration controller, in addition to the case of the attitude control only, the modal coordinate vector is needed for the control, and the modal coordinate vector can be provided by the displacement or strain sensors in the flexible structures.

4. Steering law design

CMGs have a singularity problem. In this section, a singularity avoidance steering law for a spacecraft with DGVSCMGs is proposed. The steering law considered in this paper is rewritten as follows:

$$\boldsymbol{u} = \overline{\boldsymbol{B}}\boldsymbol{u}'. \tag{59}$$

To obtain the actuator input $\boldsymbol{u}'$, the inverse matrix of $\overline{\boldsymbol{B}}$ is considered.

4.1. Moore-Penrose steering law

The general solution of Eq. (59) is given by

$$\boldsymbol{u}' = \overline{\boldsymbol{B}}^{\dagger}\boldsymbol{u}, \tag{60}$$

with

$$\overline{\boldsymbol{B}}^{\dagger} = \overline{\boldsymbol{B}}^T(\overline{\boldsymbol{B}}\overline{\boldsymbol{B}}^T)^{-1}. \tag{61}$$

This steering law, known as the "Moore-Penrose steering law", is often used. However, this steering law can not avoid CMG singularities.

4.2. Singularity robustness steering law

To avoid these singularities, a singularity robustness (SR) steering law [19] is proposed as follows:

$$\boldsymbol{u}' = \overline{\boldsymbol{B}}^{\sharp}\boldsymbol{u}, \tag{62}$$

with

$$\overline{\boldsymbol{B}}^{\sharp} = \overline{\boldsymbol{B}}^T(\overline{\boldsymbol{B}}\overline{\boldsymbol{B}}^T + \alpha\boldsymbol{I}_3)^{-1}, \tag{63}$$

where α is an SR parameter that is a positive scalar to be properly selected. In this paper, a sigmoid function as an SR parameter is introduced as follows:

$$\alpha = \kappa\frac{1 - \exp\left(-\frac{1}{m}\right)}{1 + \exp\left(-\frac{1}{m}\right)}, \tag{64}$$

with a singularity measurement

$$m = \sqrt{\det(\overline{\boldsymbol{B}}\overline{\boldsymbol{B}}^T)}, \tag{65}$$

when m is close to 0, the system falls into the singularity. The parameter κ is a positive scalar. Although the control input can be calculated by using this SR steering law, it is not guaranteed to steer gimbal angles away from their singularities.

4.3. SR steering law with null motion

To steer gimbal angles away from their singularities, an SR steering law with null motion coming from a redundancy in a DGVSCMG system is proposed. A general solution of an SR steering law includes two terms constructed by the particular solution and the homogeneous solution as follows:

$$\boldsymbol{u}' = \overline{\boldsymbol{B}}^{\sharp}\boldsymbol{u} + \overline{\boldsymbol{W}}\boldsymbol{N} \tag{66}$$

with

$$\boldsymbol{W}' = \text{diag}\{w_1, ..., w_6\}, \quad w_i > 0, \quad 1 \le i \le 6, \tag{67}$$

$$\boldsymbol{N} = [\boldsymbol{I}_6 - \overline{\boldsymbol{B}}^{\sharp}\overline{\boldsymbol{B}}]\,\boldsymbol{t}, \quad \boldsymbol{t} \in \mathbf{R}^6 \tag{68}$$

where the matrix $\boldsymbol{N}$ is the kernel space of $\overline{\boldsymbol{B}}$ and $\overline{\boldsymbol{W}}$ is the weighting matrix. When $\boldsymbol{t} \neq 0$, the term $\overline{\boldsymbol{W}}'\boldsymbol{N}$ in Eq. (66) provides null motion of the DGVSCMG steering law. To steer gimbal angles toward a preferred configuration, the vector $\boldsymbol{t}$ is determined by

$$\boldsymbol{t} = \overline{\boldsymbol{u}}^* - \overline{\boldsymbol{u}} \tag{69}$$

where $\overline{\boldsymbol{u}} = [\boldsymbol{\Omega}^T\ \boldsymbol{\delta}_i^T\ \boldsymbol{\delta}_o^T]^T$ is the actuator parameter set vector. The desired actuator parameter set vector $\overline{\boldsymbol{u}}^*$ is approximately selected to realize a desired configuration and to avoid wheel saturation. By using this steering law, the control input can be calculated, and the gimbal angles can be steered toward a preferred configuration away from singularities. In this paper, the steering law in Eq. (66) with Eqs. (68) and (69) is adopted.

5. Numerical simulation

This section presents the attitude maneuver numerical simulations by using the attitude controller in Eq. (37) and combined attitude and vibration controller in Eq. (57). As an example of a flexible spacecraft, the thermoelectric outer planet spacecraft (TOPS) as shown in Fig. 5 is considered [1]. The flexible parameters characterizing TOPS are represented by the following coupling matrix $\boldsymbol{Q}$ in $\text{Kg}^{1/2}\text{m}$, damping matrix $\boldsymbol{C}$ and stiffness matrix $\boldsymbol{D}$:

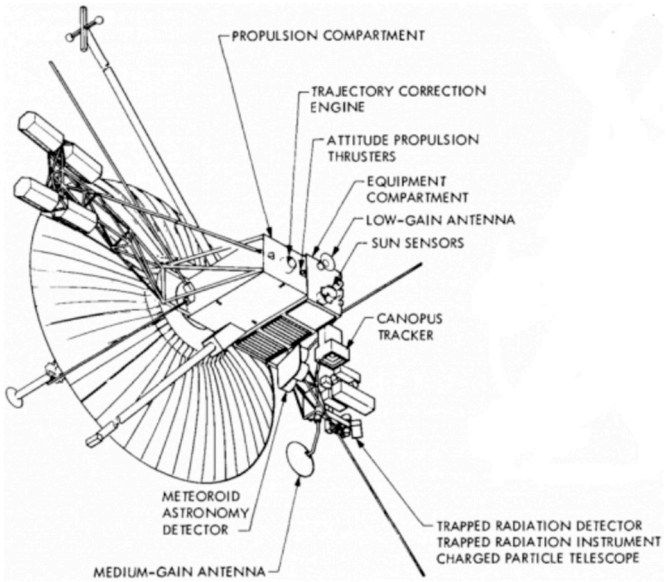

Fig. 5. TOPS by NASA [1].

$$\boldsymbol{Q} = \begin{bmatrix} -9.4733 & -15.5877 & 0.0052 \\ -0.5331 & 0.4855 & 18.0140 \\ 0.5519 & 4.5503 & 16.9974 \end{bmatrix} \tag{70}$$

$$\boldsymbol{C} = \begin{bmatrix} 0.0059 & 0 & 0 \\ 0 & 0.0075 & 0 \\ 0 & 0 & 0.0097 \end{bmatrix} \tag{71}$$

$$\boldsymbol{D} = \begin{bmatrix} 0.5476 & 0 & 0 \\ 0 & 0.5625 & 0 \\ 0 & 0 & 0.5776 \end{bmatrix}, \tag{72}$$

with the natural frequency in rad/s

$$\omega_{n1} = 0.7400,\ \omega_{n2} = 0.7500,\ \omega_{n1} = 0.7600, \tag{73}$$

and the modal dampings

$$\zeta_1 = 0.0040,\ \zeta_2 = 0.0050,\ \zeta_3 = 0.0064 \tag{74}$$

associated to the first 3 natural modes ($m = 3$). Inertia tensor ${}^{\mathcal{B}}[I_s]$ is given by

$${}^{\mathcal{B}}_{[I_s]} = \begin{bmatrix} 1543.9 & -2.3 & -2.8 \\ -2.3 & 471.6 & -35 \\ -2.8 & -35 & 1713.3 \end{bmatrix} \text{kg·m}^2. \tag{75}$$

The initial modal coordinate vector and the time derivative of the modal coordinate vector is $\eta(0) = [0\ 0\ 0]^T$, $\dot{\eta}(0) = [0\ 0\ 0]^T$, respectively.

The DGVSCMGs' parameters are given in Table 1. The wheel saturation in DGVSCMG is $\Omega = \pm 500$rad/s and the limits of the wheel input is $\dot{\Omega} = \pm 5$rad/s^2. The limits of the inner/outer gimbal input is $\dot{\delta}_{i/o} = \pm 1$ rad/s.

The disturbance torque [21] experienced by aerodynamics, solar pressure, magnetic torque, and other environmental factors is assumed to be

Table 1
DGVSCMGs' parameters.

Parameter	Value	Unit
$\mathcal{G}_{i[I_{ws}]}$	diag[0.0042 0.0042 0.0042]	kgm^2
$\mathcal{G}_{i[I_{gi}]}$	diag[0.001 0.001 0.001]	kgm^2
$\mathcal{G}_{o[I_{go}]}$	diag[0.001 0.001 0.001]	kgm^2
$\boldsymbol{\Omega}(0)$	[200 300]	rad/s
$\delta_i(0)$	[0 0]	rad
$\delta_o(0)$	$[\pi/4\ \pi/2]$	rad

$$\boldsymbol{L} = \begin{bmatrix} 4 \times 10^{-6} + 2 \times 10^{-6}\sin(nt) \\ 6 \times 10^{-6} + 3 \times 10^{-6}\sin(nt) \\ 3 \times 10^{-6} + 3 \times 10^{-6}\sin(nt) \end{bmatrix} \text{N·m}, \tag{76}$$

where n rev/day denotes the orbital frequency. A near-polar orbital satellite is considered in this simulation [22] in this case, $n = 14.57788549$.

The controller design parameters $\boldsymbol{C}'_e$ and $\boldsymbol{D}'_e$ of the GS controller for the 3-axis attitude control in Eq. (37) and the disturbance coefficient matrix $\boldsymbol{E}_e$ are given as follows:

$$\overline{\boldsymbol{C}}_e = \begin{bmatrix} 10 \times \boldsymbol{I}_3 & \boldsymbol{0}_{3\times3} \\ \boldsymbol{0}_{3\times3} & 2 \times \boldsymbol{I}_3 \\ \boldsymbol{0}_{3\times3} & \boldsymbol{0}_{3\times3} \end{bmatrix}, \quad \overline{\boldsymbol{D}}_e = \begin{bmatrix} \boldsymbol{0}_{6\times3} \\ 0.01 \times \boldsymbol{I}_3 \end{bmatrix}, \quad \boldsymbol{E}_e = \begin{bmatrix} \boldsymbol{I}_3 \\ \boldsymbol{0}_{3\times3} \end{bmatrix}, \tag{77}$$

the scheduling parameters are given in $-700 \le \rho_i \le 700,\ i = 1,\ 2,\ 3$. The controller design parameters $\widetilde{\boldsymbol{C}}'_e$ and $\widetilde{\boldsymbol{D}}'_e$ of the vibration controller in Eq. (51) and the disturbance coefficient matrix $\widetilde{\boldsymbol{E}}_e$ are given as follows:

$$\widetilde{\boldsymbol{C}}_e = \begin{bmatrix} \boldsymbol{I}_3 & \boldsymbol{0}_{3\times3} \\ \boldsymbol{0}_{3\times3} & \boldsymbol{I}_3 \\ \boldsymbol{0}_{3\times3} & \boldsymbol{0}_{3\times3} \end{bmatrix}, \quad \widetilde{\boldsymbol{D}}_e = \begin{bmatrix} \boldsymbol{0}_{6\times3} \\ \boldsymbol{I}_3 \end{bmatrix}, \quad \widetilde{\boldsymbol{E}}_e = \begin{bmatrix} \boldsymbol{I}_3 \\ \boldsymbol{0}_{3\times3} \end{bmatrix}, \tag{78}$$

the weighting matrix of the combined attitude and vibration controller $\boldsymbol{W}$ is given by

$$\overline{\boldsymbol{W}} = \begin{bmatrix} 0.06 & 0 & 0 \\ 0 & 0.06 & 0 \\ 0 & 0 & 0.06 \end{bmatrix}. \tag{79}$$

Steering law to avoid the singularities in Eq. (66) with Eqs. (68) and (69) is adapted. The design parameter for the steering law is as follows:

$$\overline{\boldsymbol{W}} = \begin{bmatrix} 1 & 0 & 0 & 0 & 0 & 0 \\ 0 & 1 & 0 & 0 & 0 & 0 \\ 0 & 0 & 10 & 0 & 0 & 0 \\ 0 & 0 & 0 & 10 & 0 & 0 \\ 0 & 0 & 0 & 0 & 10 & 0 \\ 0 & 0 & 0 & 0 & 0 & 10 \end{bmatrix}, \quad \varkappa = 10, \quad \widetilde{\boldsymbol{u}}^* = [250\ 250\ 0\ 0\ 0\ \pi/2]^T \tag{80}$$

In this paper, the gain of the weighting matrices in Eqs. (79) and (80) are determined by trial and error.

5.1. Large maneuver simulation

In this subsection, the large attitude maneuver is considered. The initial/desired attitude parameter and the angular velocity are given in Table 2. This maneuver [11] corresponds to a rotation in Eq. (20) as follows:

$$\hat{\boldsymbol{\alpha}} = [-2/\sqrt{14}\ \ 1/\sqrt{14}\ \ 3/\sqrt{14}\,]^T \tag{81}$$

$$\Theta = 8/9\pi \tag{82}$$

This maneuver rotates the spacecraft 160° around the principal rotation axis $\hat{\boldsymbol{\alpha}}$. This simulation also considers the model uncertainty $\Delta[J]$ on the inertia tensor $[J]$. Therefore in the numerical simulation, the inertia tensor $[J]$ is given by $[J] + \Delta[J]$ with $\Delta[J] = 0.2[J]$, since the oscillation of the flexible solar battery paddles or flexible parabolic communication antenna prevent the spacecraft inertia tensor from

Table 2
Attitude simulation parameters.

Parameter	Value	Unit
$\boldsymbol{q}(0)$	$[0\ 0\ 0\ 1]^T$	–
$\boldsymbol{q}_d$	$[-0.5264\ \ -0.2632\ 0.7896\ 0.1736]^T$	–
$\omega(0)$	$[[0.06\ 0.05\ \ -0.08]^T$	rad/s
ω_d	$[0\ 0\ 0]^T$	rad/s

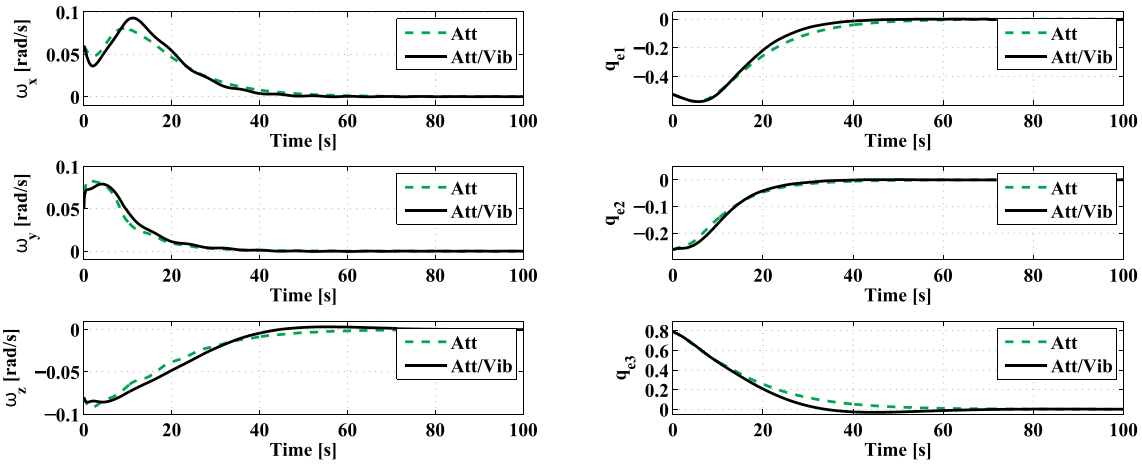

(a) Angular velocity. (b) Vector part of the quaternions.

Fig. 6. Spacecraft attitude motion.

being known exactly in a practical situation. This inertia tensor variation can heavily affect spacecraft attitude, which invariably presents a challenge to the spacecraft attitude control system [12].

Figs. 6–8 show the comparison of the simulation results by using two controllers. Black lines and green lines show the simulation results by using the GS attitude controller in Eq. (37) that only considers attitude control and the combined attitude and vibration controller in Eq. (57) that considers both attitude and vibration control, respectively.

The time history of the angular velocity of a spacecraft and attitude parameters (quaternions) are shown in Fig. 6. From this figure, the 3-axis attitude control have been completely attained. Fig. 8 shows the time history of the modal vector. This figure demonstrates the effectiveness of the proposed combined attitude and vibration controller, since the response of the modal displacements is improved and the maximum amplitude value of the result by proposed controller is less than half of that by the attitude controller. Fig. 8 shows controller input results. This figure shows the amount of control input coming from proposed controller is almost the same as attitude controller.

Figs. 9 and 10 show the simulation results of the DGVSCMG

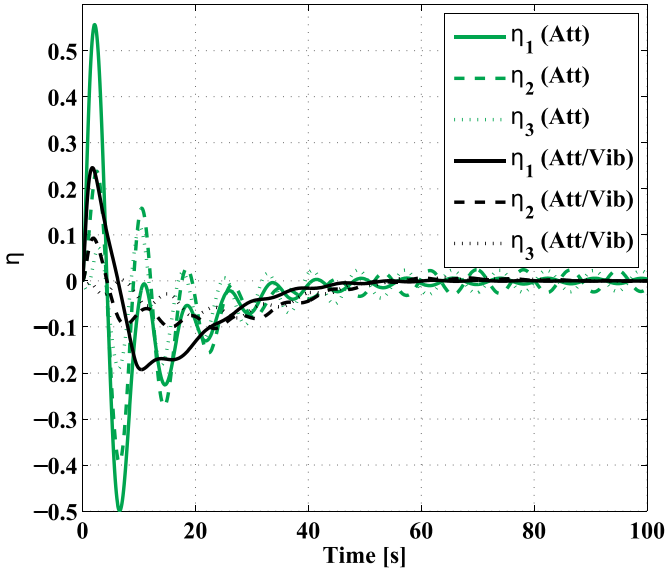

Fig. 7. Modal.

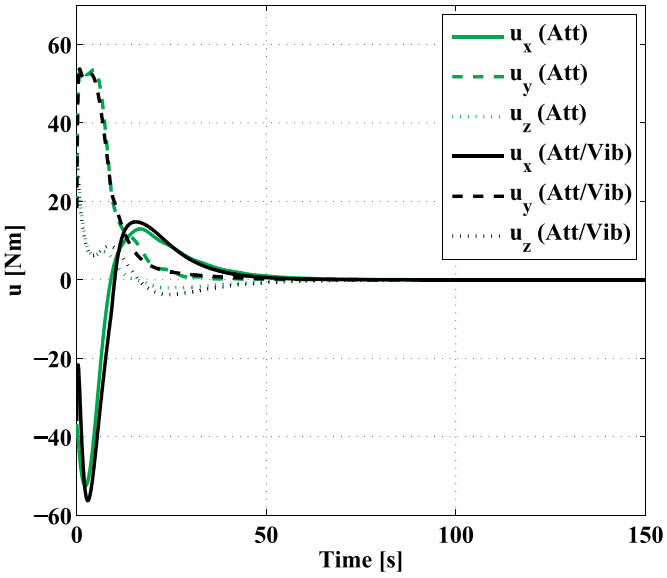

Fig. 8. Controller input.

rotational motion by using the singularity avoidance steering law in Eq. (66). Subfigures (a) and (b) in Fig. 9 show the wheel input and the gimbal input, respectively. From these subfigures, DGVSCMG input does not exceed limit by the torque limiter. Wheel and gimbal motion in subfigures (c) and (d) in Fig. 9 show that the wheel angular velocity and the gimbal angles converge to the preferred DGVSCMG parameter set $\tilde{\boldsymbol{u}}^*$ and also the singularity measurement (when m is close to 0, the system falls into the singularity) go away from the singularity statement as in Fig. 10.

5.2. Monte Carlo simulation of the rest-to-rest maneuver

In this subsection, a monte carlo (MC) simulation of a rest-to-rest maneuver is considered, which is the initial attitude parameter $\boldsymbol{q}(0) = [0\ 0\ 0\ 1]^T$ and initial/desired angular velocity $\boldsymbol{\omega}(0) = [0\ 0\ 0]^T$ rad/s, $\boldsymbol{\omega}_d = [0\ 0\ 0]^T$ rad/s. The desired attitude parameter $\boldsymbol{q}_d$ can be represented by the spherical coordinate system as follows:

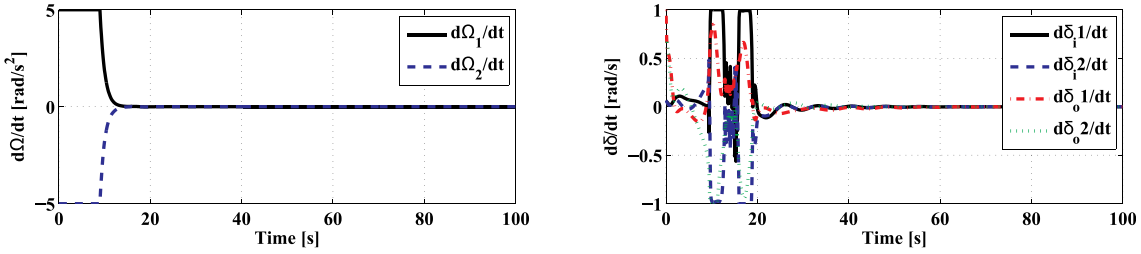

(a) Wheel acceleration (wheel input).

(b) Gimbal rates (gimbal input).

(c) Wheel spin rates.

(d) Gimbal angles.

Fig. 9. DGVSCMGs' rotation.

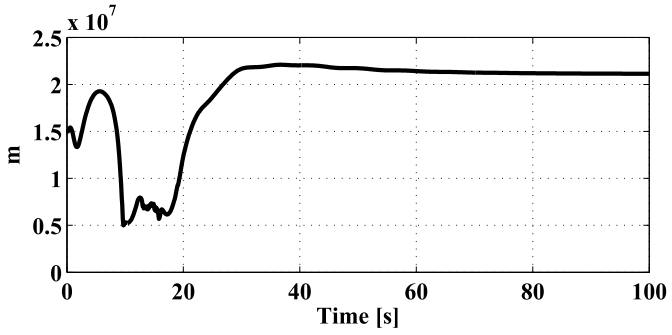

Fig. 10. Singularity measurement.

$$\hat{\alpha} = \begin{bmatrix} \sin\theta\cos\phi \\ \sin\theta\sin\phi \\ \cos\theta \end{bmatrix} \tag{83}$$

Note that the parameters θ and ϕ represent the angular coordinates as in Fig. 11. In this MC simulation, 614 (θ, ϕ) sets $(0 \le \theta \le 180,\ 0 \le \phi \le 360$ deg) of the combination at 10 deg intervals are adopted. The other simulation parameters are analogous to the parameters as in Subsection 5.1. Table 3 shows the 614-run mean values of the vibration function J_η for the modal of the vibration as follows:

$$J_\eta(t) = \int_0^{t_f} \tilde{\boldsymbol{x}}^T \tilde{\boldsymbol{x}}\, d\tau \quad \tilde{\boldsymbol{x}} = [\dot{\boldsymbol{\eta}}^T\ \boldsymbol{\eta}^T]^T \tag{84}$$

Note that the terminating time t_f of the J_η norm is considered as 200 s simulation time. Figs. 12 and 13 show the 10, 90 and 180° rotation simulation results by using the attitude controller and the proposed attitude and vibration controller, respectively. These figures show vibration surfaces, where the direction of the vector from the origin of the coordinate axes to the surface represents the direction of the principal rotation axis $\hat{\alpha}$ in Eq. (83), and the magnitude of the vector represents the value of the vibration function in Eq. (84) as in Fig. 11.

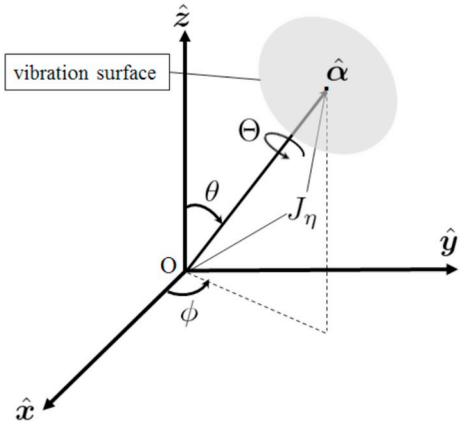

Fig. 11. MC simulation.

Table 3
Mean values of the vibration function.

	Att controller	Att/Vib controller
Θ= 10 deg	5.2621×10^2	0.2599
Θ= 90 deg	5.4831×10^2	2.0979
Θ= 180 deg	5.5597×10^2	4.7161

From Figs. 12 and 13, when the rotation is large, the vibration surface swell outward in the ± y direction of the principal rotation axis $\hat{\alpha}$ and the shapes are almost symmetric with respect to the y axis. This

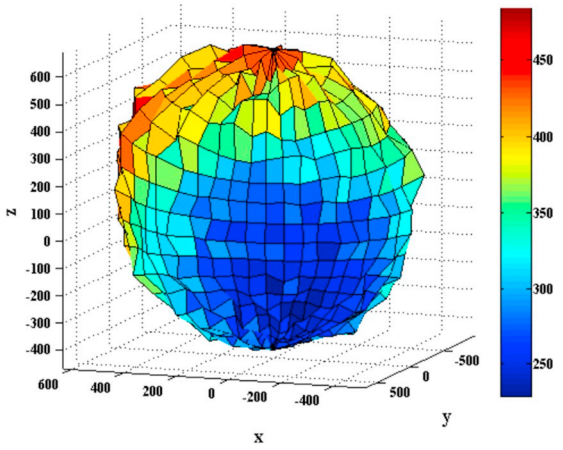

(a) MC result (Θ = 10 deg)

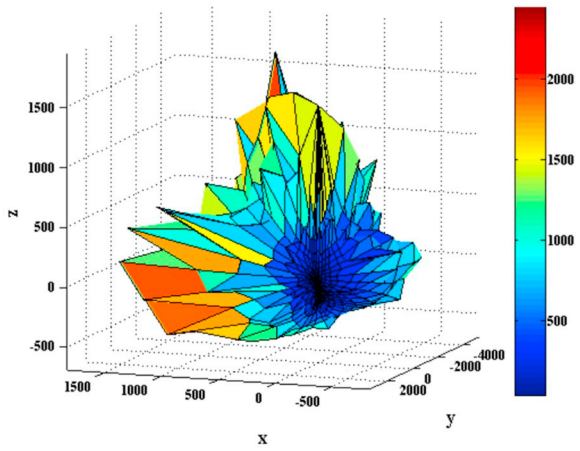

(b) MC result (Θ = 90 deg)

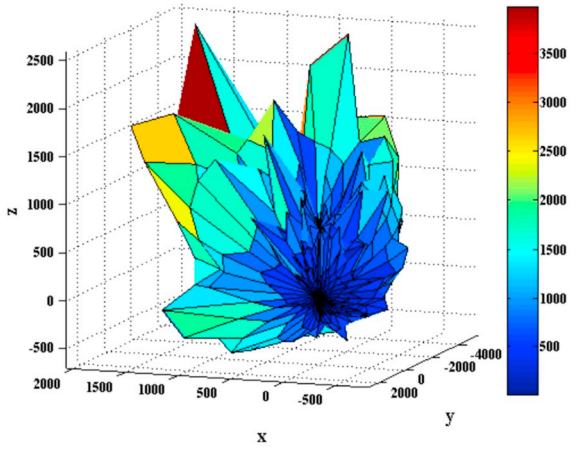

(c) MC result (Θ = 180 deg)

Fig. 12. Vibration surface (Att).

means the rotation around the y axis causes a large vibration in this TOPS spacecraft. This generally depends on the spacecraft parameters such as inertia tensor $[\boldsymbol{J}]$, the coupling matrix $\boldsymbol{Q}$ the set of actuator, and the simulation parameters such as the initial wheel spin rates and gimbal angles of the DGVSCMGs. The volume of the vibration surfaces for the attitude and vibration controller is less than that for the attitude controller and the surfaces by the proposed controller are bounded and very smooth. From Table 3, the oscillation of a flexible spacecraft by using the proposed attitude and vibration controller is also suppressed 100 times less than that by using the attitude controller. These results imply that rest-to-rest maneuver at any rotation around an arbitrary axis are successfully achieved while suppressing the oscillations by the controller in Eq. (57). Therefore, the effectiveness of the proposed attitude and vibration controller is demonstrated from these MC simulations.

6. Conclusion

In this paper, the dynamics and the linear parameter-varying (LPV) model of a flexible spacecraft equipped with multiple double-gimbal variable-speed control moment gyros (DGVSCMGs) are explored and developed, respectively. A gain-scheduled (GS) controller for 3-axis attitude control is designed by the post-guaranteed linear matrix inequalities (LMIs) method with $\mathbf{H}_2/\mathbf{H}_\infty$ constraints. Based on the dynamic inversion (DI) technique, a combined controller for attitude and vibration control is obtained. To avoid the singularity problem of DGVSCMGs, a singularity robustness (SR) steering law with null motion is applied with a sigmoid function as an SR parameter. Monte Carlo (MC) simulations demonstrate that the volume of the vibration surface for the combined controller is less than that for the attitude controller. Future work will consider translational motion of the center of mass of

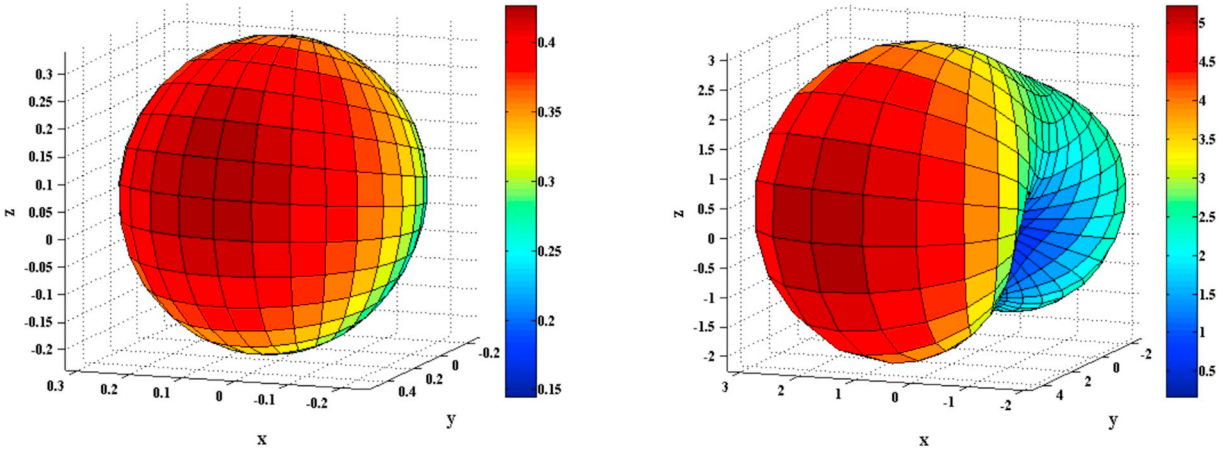

(a) MC result (Θ = 10 deg)

(b) MC result (Θ = 90 deg)

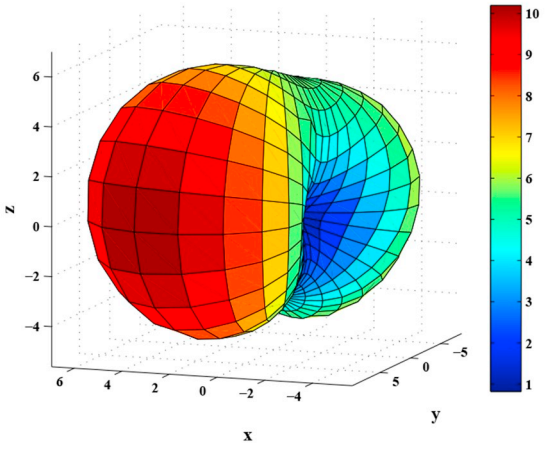

(c) MC result (Θ = 180 deg)

Fig. 13. Vibration surface (Att/Vib).

the flexible structures and a gain tuning method for the combined attitude and vibration controller and the singularity avoidance steering law.

Acknowledgment

This work was supported by JSPS Grant-in-Aid for Scientific Research Grant Numbers 15J11371 and (C)15K06149.

References

[1] E.L. Divity, R.F. Draper, H.K. Frewing, W. Stavro, TOPS spacecraft and the missions, Astronaut. Aeronaut. 8 (1970) 45–54.
[2] P.W. Likins, G.E. Fleischer, Results of flexible spacecraft attitude control studies utilizing hybrid coordinates, J. Spacecraft Rockets 8 (3) (1971) 264–273.
[3] T. Ohtani, Y. Hamada, T. Nagashio, T. Kida, S. Mitani, I. Yamaguchi, T. Kasai, H. Igawa, Robust attitude control using Mu-synthesis for the large flexible satellite ETS-VIII, J. Space Technol. Sci. 25 (1) (2011) 27–40.
[4] R. Dodge, M.A. Boyles, C.E. Rasbach, Key and driving requirements for the Juno payload suite of instruments, Proceedings of AIAA SPACE 2007 Conference & Exposition, AIAA 2007-6111, 2007 Long Beach, CA.
[5] R.S. Grammier, A look inside the Juno mission to Jupiter, Proceedings of 2009 IEEE Aerospace Conference, IEEE AC paper #1582, 2009 Big Sky, MT.
[6] P. Apkarian, P. Gahinet, G. Becker, Self-scheduled $\mathbf{H}_\infty$ control of linear parameter-varying systems: a design example, Automatica 31 (9) (1995) 1251–1261 September.
[7] P.P. Khargonekar, M.A. Rotea, $\mathbf{H}_2/\mathbf{H}_\infty$ control: a convex optimization approach, IEEE Trans. Automat. Contr. 36 (7) (1991) 824–837.
[8] E. Feron, P. Apkarian, P. Gahinet, Analysis and synthesis of robust control systems via parameter-dependent Lyapunov functions, IEEE Trans. Automat. Contr. 41 (7) (1996) 1041–1046.
[9] P. Gahinet, P. Apkarian, M. Chilali, Affine parameter-dependent Lyapunov functions and real parametric uncertainty, IEEE Trans. Automat. Contr. 41 (3) (1996) 436–442.
[10] T. Shimomura, T. Kubotani, Gain-scheduled control under common Lyapunov functions: conservatism revisited, Proc. of 2005 American Control Conference, 2005, pp. 870–875.
[11] S. Di Gennaro, Passive attitude control of flexible spacecraft from quaternion measurements, J. Optim. Theor. Appl. 116 (1) (2003) 41–60.
[12] Q. Hu, Sliding mode maneuver control and active vibration damping of three-axis stabilized flexible spacecraft with actuator dynamics, Nonlinear Dynam. 52 (2008) 227–248.
[13] J. Reiner, G.J. Balas, W.L. Garrard, Robust dynamic inversion for control of highly maneuverable aircraft, J. Guid. Contr. Dynam. 18 (1) (1995) 18–24 January-February.

[14] D. Ito, D. Ward, J. Valasek, Robust dynamic inversion controller design and analysis for the X-38, Proceedings of AIAA Guidance, Navigation, and Control Conference, AIAA 2001-4380, 2001 Montreal, Canada.
[15] M.B. McFarland, C.N. D'Souza, Missile flight control with dynamic inversion and structured singular value synthesis, Proceedings of AIAA Guidance, Navigation, and Control Conference, AIAA 94-3604-CP, 1994.
[16] J.H. Ryu, C.S. Park, M.J. Tahk, Plant inversion control of tail-controlled missiles, Proceedings of AIAA Guidance, Navigation, and Control Conference, AIAA 97-3766, 1997.
[17] P. Cui, J. He, Steering law for two parallel variable-speed double-gimbal control moment gyros, J. Guid. Contr. Dynam. 37 (1) (2014) 350–359 January-February.
[18] T. Sasaki, T. Shimomura, Fault-tolerant architecture of two parallel double-gimbal variable-speed control moment gyros, Proceedings of AIAA Guidance, Navigation, and Control Conference, AIAA 2016-0090, 2016 San Diego, CA.
[19] B. Wie, D. Bailey, C. Heiberg, Singularity robust steering logic for redundant single-gimbal control moment gyros, J. Guid. Contr. Dynam. 24 (5) (2001) 865–872 September-October.
[20] S. Kwon, T. Shimomura, H. Okubo, Pointing control of spacecraft using two SGCMGs via LPV control theory, Acta Astronaut. 68 (7–8) (2011) 1168–1175. April-May.
[21] M. Sidi, Spacecraft Dynamics and Control, a Practical Engineering Approach, Cambridge Univ. Press, New York, 1997, pp. 241–242.
[22] C.E. Fossa, R.A. Raines, G.H. Gunsch, M.A. Temple, An overview of the IRIDIUM low earth orbit (LEO) satellite system, Proceedings of the IEEE National Aerospace and Electronics Conference, Inst. of Electrical and Electronics Engineers, Piscataway, NJ, 1998, pp. 152–159.